



# Energy response of an imaging plate exposed to standard beta sources

A.L. Gonzalez<sup>a,\*</sup>, H. Li<sup>a</sup>, M. Mitch<sup>b</sup>, N. Tolc<sup>c</sup>, D.M. Duggan<sup>a</sup>

<sup>a</sup> Department of Radiation Oncology, Vanderbilt University, The Vanderbilt Clinic, B-902, 1301 22nd Avenue South, Nashville, TN 37232-5671, USA

<sup>b</sup> Ionizing Radiation Division, National Institute of Standard and Technology, 100 Bureau Drive, Stop 8460, Gaithersburg, MD 20899-8460, USA

<sup>c</sup> Department of Physics and Astronomy, Vanderbilt University, Stevenson Center, 6301, Nashville, TN 37235, USA

Received 1 March 2002; received in revised form 13 June 2002; accepted 2 July 2002

## Abstract

Imaging plates (IPs) are a reusable media, which when exposed to ionizing radiation, store a latent image that can be read out with a red laser as photostimulated luminescence (PSL). They are widely used as a substitute for X-ray films for diagnostic studies. In diagnostic radiology this technology is known as computed radiography. In this work, the energy response of a commercial IP to beta-particle reference radiation fields used for calibrations at the National Institute of Standards and Technology was investigated. The absorbed dose in the active storage phosphor layer was calculated following the scaling procedure for depth dose for high  $Z$  materials with reference to water. It was found that the beta particles from Pm-147 and Kr-85 gave 68% and 24% higher PSL responses than that induced by Sr-90, respectively, which was caused by the different PSL detection efficiencies. In addition, normalized response curves of the IPs as a function of depth in polystyrene were measured and compared with the data measured using extrapolation chamber techniques. The difference between both sets of data resulted from the continuous energy change as the beta particle travels across the material, which leads to a different PSL response.

© 2002 Elsevier Science Ltd. All rights reserved.

**Keywords:** Imaging plates; Beta emitters; Photostimulable phosphor; Brachytherapy

## 1. Introduction

New brachytherapy sources have been developed as potential solutions for the treatment of post-intervention restenosis (Soares et al., 1998; Janicki et al., 1999). Some of the catheter-based systems, radioactive stents, and radioactive liquids use beta emitters such as P-32 and Sr-90 due to the advantages of short range dose delivery and suitable half-lives. As in other types of brachytherapy, the dose rate distributions must be thoroughly mapped at all the relevant distances. For example,

according to the recommendations of Task Group 60 of the American Association of Physicists in Medicine (AAPM), the uniformity along the catheter axis at a radial distance of 2 mm should be uniform to within  $\pm 10\%$  in the center two-thirds of the treated length (Nath et al., 1999). Dosimetric assessment of clinical sources may be very difficult due to the different source geometries. The low activities associated with radioactive stents present additional dosimetric difficulties. Radiochromic film dosimetry has been used extensively for some of these sources (Meigooni et al., 1996; Reinstein et al., 1997; Zhu et al., 1997). However, a major disadvantage is the insensitivity of radiochromic film, which results in a rather lengthy irradiation time. Regular X-ray film could also be used to assess the dose distribution from these sources, but they still have the

\*Corresponding author. Tel.: 615-322-2555; fax: 615-343-0161.

E-mail addresses: albin.l.gonzalez@vanderbilt.edu (A.L. Gonzalez), hui.li@mcm.vanderbilt.edu (H. Li).

disadvantage of lower sensitivity than imaging plates (IPs) due to higher noise level, and any variation in the development process would add more uncertainty to the reading when the film is scanned with a densitometer. Radiochromic film and regular X-ray film are, therefore, not very practical for use as an on-site clinical tool for quality assurance of low-dose-rate radioactive implants.

Fig. 1 shows a comparison of the dose profile of a novel P-32 coated stent measured using radiochromic film to the response profile of an IP. The measurement of the response of the IP was done in a period of 15 min, following a 30-day irradiation time in a tissue equivalent phantom with a stack of radiochromic film. The activity was about four times less when using the IP. However, the response was sufficient to show that the stent did not meet the AAPM recommendation for uniformity.

Given the above motivation, the purpose of this study is to test the suitability of the IPs as dosimeters for quality assurance of low-activity brachytherapy beta sources such as Sr-90 beads and some of the sources used in radio-immuno assays. In this work, the first calibration curves of IPs to the national standard beta sources at NIST were obtained.

The IP commonly used for computed radiography and bio-imaging is a film-like sensor comprised of specifically designed phosphors (typically  $\text{BaF-Br}_{0.85}\text{I}_{0.15}:\text{Eu}^{2+}$  which is embedded in a binder) that can absorb and store radiation energy in the form of defect centers in the crystal lattice (Amemiya and Miyahara, 1988; Winnacker, 1993). The stored energy in these storage centers is stable until scanned with a red laser beam (632.8 nm), which releases the energy via photo stimulation as blue (390 nm) luminescence light that is collected by a photomultiplier tube (PMT). IPs have outstanding characteristics including very high

sensitivity, a wide dynamic range of linear response to dose of about five orders of magnitude, high resolution and direct digitization of the image. The plates are erased with white light after they are read with the laser, so they are reusable. The response of the plates is expressed in units of  $\text{PSL}/\text{mm}^2$ .

In this study, the photostimulated luminescence (PSL) response per absorbed dose in the phosphor layer was investigated for three beta sources. It was found that different calibration curves are needed for different beta sources, which resulted from different depth-dose distribution profiles and consequent different detection efficiencies of PSL photons. This energy-dependent behavior led to the difference between IP and extrapolation chamber (EC) for measurement of normalized response curves as a function of depth in polystyrene.

## 2. Materials and methods

The IP used in this work is the Fuji BASIII N (Fujifilm Medical Systems USA, Inc. Stamford, CT). The active layer is about  $139\ \mu\text{m}$ . The scanner used in this study was a Fuji BAS 2000. It was programmed with the following parameters: size =  $20 \times 25\ \text{cm}^2$ , sensitivity = 10,000, gradation = 1024 and resolution =  $200\ \mu\text{m}$ .

The beta secondary standards system (BSS2) with the corresponding standard beta sources was used in this investigation. The sources are placed in a specially designed mounting in the form of a cross. A computer controlled shutter opens for the desired time for the exposure. The shutter will not open unless the measurement distance and the beta source are matched. This feature limits undesired exposure due to errors in the

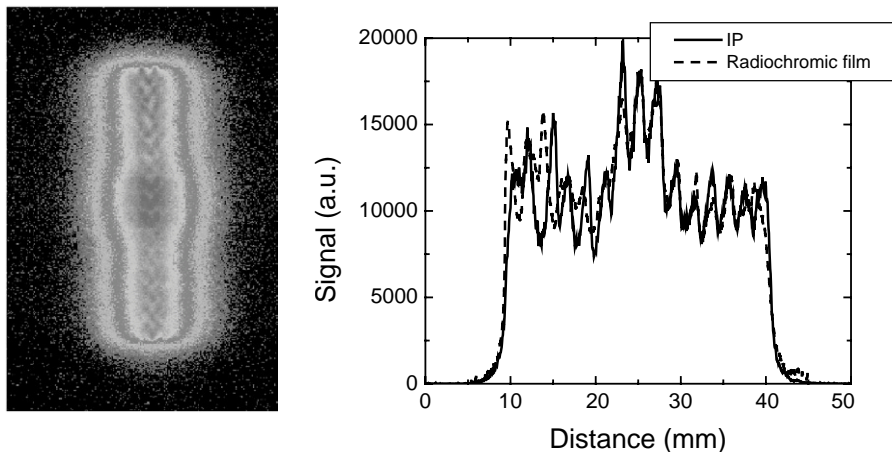


Fig. 1. (a) Image of the relative dose distribution of the stent using IP at a plane parallel to the stent axis and in contact with the stent. (b) Profiles of the dose distribution along the central axis of the stent using IPs (exposure: 15 min) and radiochromic film (exposure: 30 days).

experimental set-up. Furthermore, pressure, temperature and humidity were measured simultaneously for all exposures since they affect the air density between the source and the detector and the beta energy spectrum as well. Because there were no significant variations in the reading of temperature, pressure and humidity during the measurements, no corrections were applied. Fig. 2 shows the experimental setup for the exposures. The plates were attached to a thick polystyrene block so that the plates were perpendicular to the axis of the beta fields. Information about the source encapsulations, photon radiations emitted, nominal activity, material of the inactive cover foils (source window), beta particle spectra, etc., is given in Pruitt et al. (1988), ISO 6980 (1996), ICRU (1997), and Ambrosi et al. (1999).

The experimental method followed was to expose the IP to three beta-particle reference radiation fields, which are used for beta particle calibrations at the National Institute of Standards and Technology (NIST). Table 1 shows the fields used as well as the corresponding calibration distances for three radionuclides: Kr-85, Pm-147 and Sr-90, which covered an energy spectrum up to 2.3 MeV in three energy ranges. Absolute dose equivalent measurements at a perpendicular skin depth of 0.07 mm as previously measured with an EC yielded known dose rates at several distances from the sources.

To study the plate response as a function of polystyrene depth, the IP was exposed to a Sr-90 source with various thicknesses of polystyrene placed on top of the plate for the same period of time. The areal density of polystyrene varied from 79 to 1200 mg/cm<sup>2</sup>. Immediately after the exposures the plate was read with the scanner. In all cases the PSL/mm<sup>2</sup> value reported here was an average over a 3 cm diameter region of interest

(ROI) in the center of the beta field image. After each reading the plate was erased using white light for approximately 10 min in order to completely remove the residual information so that the plate could be reused for the next exposure. In all cases the same exposure was repeated twice and the values of PSL/mm<sup>2</sup> reported here are the average.

### 3. Results and discussion

Since the purpose of this work is to study the suitability of the IPs as a dosimeter for beta sources, it is important to investigate how the dose is distributed in the phosphor layer. The active phosphor layer includes high atomic number elements. The scaling procedure for depth dose for high Z materials with reference to water was followed (Cross, 1968; ICRU, 1997; Marcu and Prestwich, 1998) in order to get the absorbed dose in the phosphor layer for each source. The data used for doing the scaling to phosphor were the normalized ionization currents in tissue depths and the known dose rates at 0.07 mm tissue depth measured by Pruitt et al. (1988) and Ambrosi et al. (1999) with the EC. Water and tissue were considered equivalent. For this work the existence of the thin protective layer of the IP (about 10 μm) was neglected. In addition, the perturbation of the dose in the phosphor layer due to the interfaces with the undercoating and the polyester base layers was ignored.

#### 3.1. Scaling method

The absorbed dose in the phosphor layer was derived from the directional dose rate equivalent  $H'(0.07, \Omega)$

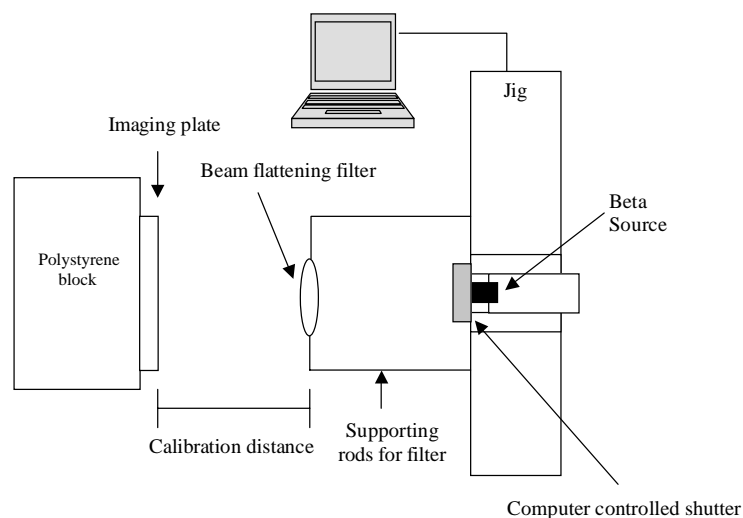


Fig. 2. Experimental setup for the exposure of the IPs. Beta sources used are Sr-90, Kr-85 or Tl-204 and Pm-147. See Table 1 for irradiations procedure specifics.

Table 1

Available standard beta sources with calibration distances and corresponding dose rates measured with an extrapolation chamber at NIST, defined at a depth of 0.07 mm in soft tissue

Isotope	Nominal activity (GBq)	Distance (cm)	Half-life (day)	Dose rate in tissue at 70 $\mu\text{m}$ ( $\mu\text{Gy/s}$ )	Average dose rate (in phosphor layer) ( $\mu\text{Gy/s}$ )
Pm-147	3.7	20	958.2	3	1.46
Kr-85	3.7	30	3915	50	46.26
Sr-90	0.46	50	10,520	6	7.77

(Pruitt et al., 1988; Ambrosi et al., 1999) in units of Sv/s measured in tissue by the EC at depth of 0.07 mm. The directional dose rate equivalent  $H'(0.07, \Omega)$  is the dose rate at a point in a specified direction  $\Omega$  in a radiation field that would be produced by the corresponding expanded field in the ICRU sphere at depth of 0.07 mm. In the present case the quality factor  $Q$  is one (ICRP, 1990) and the range of the beta particles is small compared to the 30 cm diameter of the ICRU sphere, so that the curvature of the ICRU sphere can be neglected and it may be treated as a slab phantom. Therefore,  $H'(0.07, 0^\circ)$  is equal to the directional absorbed dose rate  $D'(0.07, 0^\circ)$  in units of Gy/s, defined as the absorbed dose rate in a slab phantom consisting of soft tissue.  $D'(0.07, 0^\circ)$  is the basic physical quantity used to quantify reference radiation fields (ISO, 6980, 1996) and is reported in the fifth column of Table 1. Using these known absorbed dose rates at 0.07 mm depth in tissue together with the measurements of the percentage depth dose in tissue with the EC (Pruitt et al., 1988; Ambrosi et al., 1999) for the same radionuclides, the absorbed dose rate as a function of tissue depth was calculated. Fig. 3 shows the depth dose rate curves in tissue for the Pm-147, Kr-85 and Sr-90 sources. The dose rate in the phosphor layer as a function of depth can then be derived using the scaling method from these curves.

Even though the depth dose measurements shown in Fig. 3 are in tissue, the same curves for the scaling procedure were used as if they were in water since the error introduced by this simplification in the calculation is small (1.5%), so for the calculation that follows tissue and water are treated as equal.

The scaling method used here (ICRU, 1997) has been shown to be a reliable procedure for estimating beta dose distributions in different media from the dose distribution in a reference medium. Water ( $w$ ) was used as the reference medium for the calculation

$$D_{\text{phosphor}}(d) = \eta_w D_w(\eta_w d). \quad (1)$$

In the above equation the depth  $d$  in  $\text{g/cm}^2$  is scaled by the factor  $\eta_w$  and the dose is normalized by the same factor in accordance with the principle of energy conservation (Marcu and Prestwich, 1998). The dose

distributions calculated with this method show very good agreement with measurements and computer simulations using Monte Carlo codes (Janicki et al., 1999; Marcu and Prestwich, 1998). The  $Z_{\text{eff}}$  for our active layer was calculated using the equation in ICRU (1997):

$$Z_{\text{eff}} = \frac{\sum_i w_i Z_i^2 / A_i}{\sum_i w_i Z_i / A_i}, \quad (2)$$

where  $Z_i$  is the atomic number of the constituent element  $i$ ,  $w_i$  is its fraction by weight and  $A_i$  its mass number. The atomic numbers used were Ba = 56, F = 9, I = 53 and Br = 35. The dopant  $\text{Eu}^{2+}$  which replaces Ba in the ionic crystal was neglected in the calculation since its concentration is about 0.1 mol%. The effective atomic number of the binder was assumed to be the same as water ( $Z_{\text{eff}} = 6.60$ ) (Li, 2001). The error introduced by this assumption is small since the dominant terms in the sum in Eq. (2) for the phosphor layer are from the high  $Z$  components. In addition, the weight fraction of the phosphor powder and the binder are  $w_{\text{phosphor}} = 89\%$  and  $w_{\text{binder}} = 11\%$  (Hopton, 2001; Li, 2001), respectively. The calculated effective atomic number is then  $42 \pm 1$ .

The scaling factor and stopping power ratios with water as the reference medium for several media of interest have been obtained empirically (Cross, 1968; Marcu and Prestwich, 1998). The following empirical relationship, valid for  $Z_{\text{eff}} > 18$ , was used for calculating the scaling factor relative to water  $\eta_w$  (Marcu and Prestwich, 1998):

$$\eta_w = 0.8254(1 + 0.0284Z_{\text{eff}})S/S_w, \quad (3)$$

where  $S/S_w$  is the stopping power of the medium relative to water. The slope was decreased by 2% as recommended by Cross for a better fit (Cross, 1968; Marcu and Prestwich, 1998). The ratio  $S/S_w$  was obtained from the expression (Marcu and Prestwich, 1998):

$$S/S_w = 2.0228 \sum [w_i Z_i / A_i (1 - \ln Z_i / 13)]. \quad (4)$$

The value calculated for our medium was  $S/S_w = 0.635$  with a corresponding scaling factor  $\eta_w = 1.225$ .

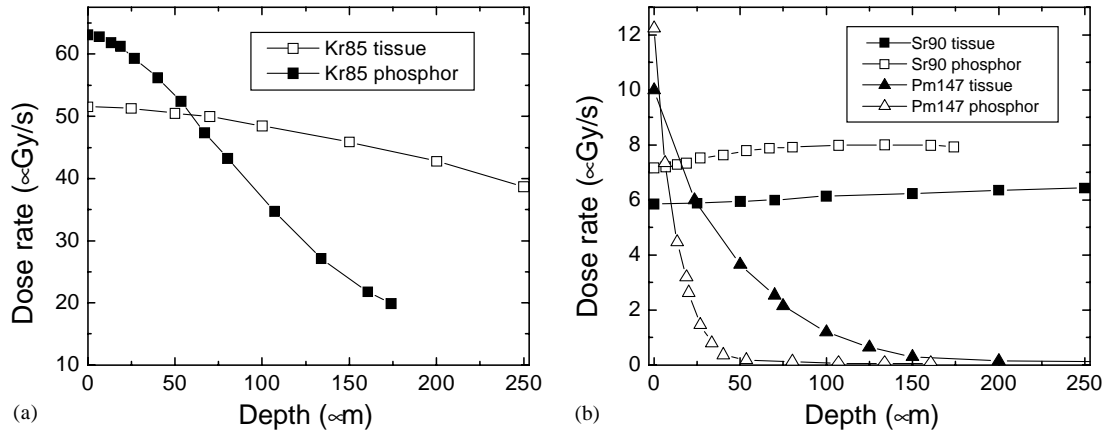


Fig. 3. Depth dose rate for the Kr-85 source in tissue and phosphor (a) and depth dose rate for the Pm-147 and Sr-90 sources in tissue and phosphor (b).

Depth dose rate curves in tissue measured by Pruitt et al. (1988) and Ambrosi et al. (1999) with an EC and the depth dose rate calculated for the phosphor layer by the above scaling method are shown in Fig. 3. Note that in the case of Pm-147 all the electrons were absorbed in the phosphor layer (139 μm). In the case of the Sr-90 source the dose is deposited almost uniformly in the phosphor layer, whereas in the case of Kr-85 the dose rate decreases rapidly with depth. From these graphs the absorbed dose rate in the whole phosphor layer was calculated as the average of the dose rate over the total thickness of the phosphor layer. These dose rates in the phosphor layer are tabulated in the last column of Table 1.

Note that the storage center concentration is a function of depth in the phosphor layer. Also note that once the depth dose rate curves are normalized for each of the sources, the curves are identical because the number of storage centers created is proportional to the deposited energy.

3.2. PSL calibration as a function of the absorbed dose in the phosphor layer

Fig. 4 shows the calibration curves of PSL/mm<sup>2</sup> versus dose absorbed in the phosphor layer for one IP and each of the three sources in the BSS2 system (Sr-90 at 50 cm). These curves were obtained by exposing the plate to each source for different periods of time covering four orders of magnitude. The slopes are listed in Table 2 (column 3) as a function of the used isotope. One can see from these slopes that the dose response for Pm-147 is about 35% and 68% higher than those for the Kr-85 and Sr-90 sources, respectively. This leads to the question: what causes this energy dependence of the PSL signal? Two mechanisms may account for it. First, the generation efficiency of the

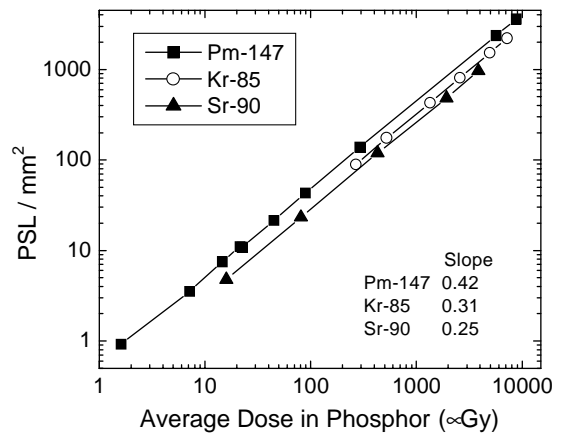


Fig. 4. PSL response as a function of the absorbed dose in the phosphor layer.

Table 2

Values of the slopes of the calibration curves from Fig. 4 and the slopes (new slope) for generated PSL photons per unit absorbed dose in total phosphor layer for three beta sources. The detection efficiencies ( $\eta_{PSL}$ ) of the PSL photons are listed in the fourth column

Isotope	$E_{max}$ (keV)	Slope	$\eta_{PSL}$	New slope
Pm-147	225	0.42	0.74	0.57
Kr-85	763	0.31	0.50	0.62
Sr-90	2284	0.25	0.43	0.58

photostimulable storage centers may depend on beta energy. Second, only a fraction of PSL photons generated in the phosphor layer are detected because many photons can not reach the IP surface where the

PMT is located due to light scattering in the polycrystalline layer. The fraction detected is dependent on the irradiation source.

### 3.3. Calculation of the PSL scattering

In order to account for the blue light scattering, the probability of escape of the PSL from the front surface of the plate was calculated as a function of the depth  $z$  of the location where the PSL was generated. This probability was deduced by assuming that the blue photons propagate by time independent diffusion (Thoms, 1996):

$$D \frac{\partial^2 n(z)}{\partial z^2} = \frac{ac}{l} n(z), \quad (5)$$

where  $D = lc(1-a)/6$  is the diffusion constant of the PSL photon in the medium,  $n(z)$  is the photon density,  $c$  is the speed of light,  $l$  is the average path length of the photon until the next uniform scattering occurs and  $a$  is the fraction of photons absorbed in the path length  $l$ . The solution to Eq. (5) gives the escape probability of the PSL from the front surface of the plate  $P_f$  (Thoms, 1996):

$$P_f(z) = \frac{1(\sqrt{a(1-a)/6} + 1/6)e^{\sqrt{6a/(1-a)}(d-z)/l} + (\sqrt{a(1-a)/6} - 1/6)e^{-\sqrt{6a/(1-a)}(d-z)/l}}{6(\sqrt{a(1-a)/6} + 1/6)^2 e^{\sqrt{6a/(1-a)}d/l} - (\sqrt{a(1-a)/6} - 1/6)^2 e^{-\sqrt{6a/(1-a)}d/l}}, \quad (6)$$

where  $d$  is the thickness of the layer  $d = 139 \mu\text{m}$ . Since the plate used in this study is similar to the STIII used in reference (Thoms, 1996) the  $l = 60 \mu\text{m}$  can be used. The fraction of blue photons absorbed  $a$  is negligible because the band gap of the crystal is much higher than the energy of the blue light (8.3 versus 3.2 eV) and the binder composition of the phosphor layer is optimized for no absorption in the spectral range of the PSL (Thoms, 1996; Li, 2001;). In this case Eq. (6) can be simplified to

$$P_f(z) = (l + d - z)/(2l + d). \quad (7)$$

The escape probability is plotted for these parameters in Fig. 5. Further, since less than 1% of the PSL signal can be obtained after a second scan we assumed that the efficiency of the photostimulation process is close to 100%, so that the calculation of the photon density distribution of laser light in the phosphor layer is not necessary. Therefore, by multiplication of the data in Fig. 5 with the depth dose in phosphor (i.e. storage center concentration) in Fig. 3 for each of the three sources, the percentage of PSL photons that could reach the PMT detector from the layer,  $\eta_{PSL}$ , was calculated, and these percentages are listed in column 4 in Table 2. Further, the slope in column 3 was divided by  $\eta_{PSL}$  in column 4 for each of the three sources to obtain the new slope listed in column 5. It can be seen that the total

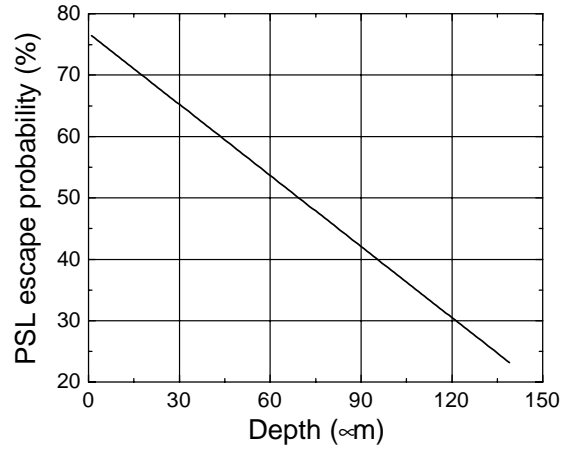


Fig. 5. Probability of PSL photons escaping as a function of depth in the phosphor layer.

numbers of PSL photons generated by the Sr-90, Kr-85 and Pm-147 sources per unit of absorbed dose are almost the same. Therefore, it may be concluded that the

different dose distribution profiles for the three beta sources together with the intrinsic scattering behavior of the PSL photons caused the significant energy dependence in the slopes of the curves in Fig. 4, which are listed in Table 2 and described in Section 3.2. It implies that the energy dependence of the generation efficiency of the photostimulable storage centers should be very small, if it exists at all. Rüter et al. (1990) demonstrated that the photostimulable storage centers could be very efficiently created by an X-ray photon with energy larger than that of the first intrinsic exciton, only 6.7 eV in the case of BaFBr:Eu<sup>2+</sup>. Therefore, since the energy transfer during an electron–electron interaction is also very efficient, it is conceivable that the number of the created photostimulable storage centers per absorbed dose is the same for all the three beta sources.

At this point, it is worth mentioning that the encapsulation of the sources used clinically will modify the original energy spectrum of the source, and the average energy, at least, is needed to make a comparison with the data of this work. This energy spectrum could be obtained either by simulation using a Monte Carlo code or direct measurement; an example of this kind of measurement is described by Pruitt et al. (1988) using a silicon surface-barrier detector.

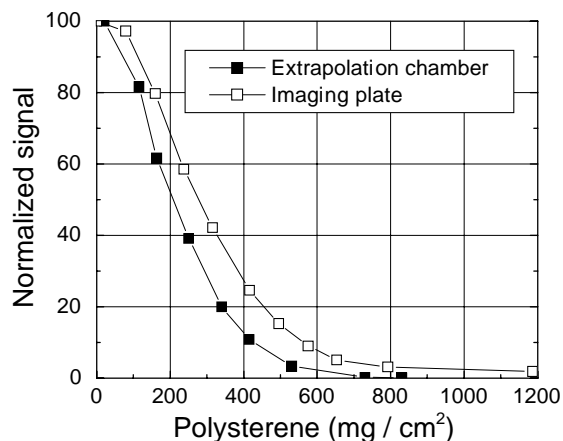


Fig. 6. Normalized PSL response and ionization current from the EC as a function of thickness in  $\text{mg}/\text{cm}^2$  of polystyrene sheets. The  $\square$  are measurements done with the IP and the  $\blacksquare$  is the ionization current carried out with the EC.

### 3.4. Comparison of the response of the IP with EC measurements

Fig. 6 illustrates the comparison of the normalized response of the IPs as a function of depth in polystyrene with analogous measurements done by Pruitt et al. (1988) using the EC. Both measurements were done using the same Sr-90 source at the same distance to the detector. It can be seen that the response curve of the IP is higher than that of the EC. This difference becomes more obvious as the density thickness of the polystyrene increases. This could be explained as follows: the energy of the beta particle decreases continuously as it travels across the polystyrene. The PSL response of the IP phosphor to a lower energy beta particle is higher than the response to a beta particle with the initial energy. By contrast, the response of the EC does not depend on the energy of beta particle, so a difference between the values measured by the two techniques, especially at greater depths, is expected.

## 4. Conclusion

Photostimulated luminescence imaging plates together with a commercial scanner are a useful tool due to their high sensitivity for measuring dose from beta sources, which is important for nondestructive measurements of sources with short half lives and low dose rates like some of those used in brachytherapy. Also, the fact that many medical centers already own a computed radiography system (used mainly for diagnostic purposes) makes this idea cost effective. In this work the

energy response of IPs containing a photostimulable high-Z phosphor material to irradiation from the standard beta sources from the NIST has been studied. The absorbed dose in the active storage phosphor layer was calculated following the scaling procedure for depth dose for high Z materials with reference to water. It was found that the PSL response to the beta particles from Pm-147 was 68% and 35% higher for the same dose absorbed in the phosphor layer than those induced by Sr-90 and Kr-85, respectively. This significant energy dependence is caused mainly by the variation of the PSL detection efficiencies for the three beta sources, whereas the possible different generation efficiencies of the photostimulable storage centers played at most a minor role. Furthermore, a difference between the normalized response curves obtained from the IPs and the EC as a function of thickness of the polystyrene buildup material was observed, which could be accounted for by the continuous reduction of the beta-particle energy in the material and consequent different PSL responses.

## Acknowledgements

The measurements for this work were done at National Institute of Standard and Technology with the help of the Radiation Interactions and Dosimetry Group. We also appreciate the help from Mr. David Hopton from Fujifilm Medical Systems USA, Inc., Stamford, CT, for giving us the technical data about the Fuji IPs and the scanner. Also we are thankful to Mr. Gary Shearer for the technical assistance at the Free Electron Center at Vanderbilt University.

## References

- Ambrosi, P., Böhm, J., Marchetto, A., Heine, U., Helmstädter, K., Soares, C., 1999. Evaluation procedure for extrapolation chamber measurements of beta radiation. PTB draft EC-project F14P960037: weakly penetrating radiations project, Germany.
- Amemiya, Y., Miyahara, J., 1988. Imaging plates illuminates many fields. *Nature* 336 (3), 89–90.
- Cross, W.G., 1968. Variation of beta dose attenuation in different media. *Phys. Med. Biol.* 13, 611–618.
- Hopton, D., 2001. Fujifilm Medical Systems USA, Inc., Stamford, CT, personal communication.
- ICRP, 1990. Recommendations of the International Commission on Radiological Protection. ICRP publication 60. *Annals of the ICRP*, Vol. 20(4). Pergamon Press, Oxford.
- ICRU, 1997. Dosimetry of external beta rays for radiation protection. ICRU Report 56, Bethesda, Maryland.
- ISO 6980, 1996. Reference beta radiations for calibrating dosimeters and dose-rate meters and for determining their response as a function of beta-radiation energy. International Standard, 2nd Edition.

- Janicki, C., Duggan, D.M., Gonzalez, A.L., Coffey, C.W., Rahdert, D., 1999. Dose model of beta-emitting stent in a realistic artery consisting of soft tissue and plaque. *Med. Phys.* 26, 2451–2460.
- Li, H., 2001. Fabrication and evaluation of storage phosphor plates for digital radiography. Ph.D. Thesis, University of Erlangen-Nürnberg, Erlangen, Germany.
- Marcu, S.M., Prestwich, W.V., 1998. Application of the scaling factor method to estimation of beta dose distributions for dissimilar media separated by a planar interface. *Med. Phys.* 25, 1478–1486.
- Meigooni, A.S., Sanders, M.I., Ibbott, G.S., Szeglin, S.R., 1996. Dosimetric characteristics of an improved radiochromic film. *Med. Phys.* 23, 1883–1888.
- Nath, R., Amols, H.L., Coffey, C.W., Duggan, D.M., Jani, S., Li, Z., Schell, M., Soares, C.G., Whiting, J.S., Cole, P.E., Crocker, I., Schwartz, R.W., 1999. Intravascular brachytherapy physics: Report of the AAPM radiation therapy committee task Group No. 60. *Med. Phys.* 26, 119–152.
- Pruitt, J.S., Soares, C.G., Ehrlich, M., 1988. Calibration of beta-particle radiation instrumentation and sources. National Bureau of Standard, Special Publication 250–21, US Department of Commerce.
- Reinstein, L.E., Gluckman, G.R., Amols, H.I., 1997. Predicting optical densitometer response as a function of light characteristics for radiochromic film dosimetry. *Med. Phys.* 24, 1935–1942.
- Rüter, H.H., von Seggern, H., Reininger, R., Saile, V., 1990. Creation of photostimulable centers in BaFBr: Eu<sup>2+</sup> single crystals by vacuum-ultraviolet radiation, physics. *Rev. Lett.* 65 (19), 87–90.
- Soares, C.G., Halpern, D.G., Wang, C.K., 1998. Calibration and characterization of beta-particle sources for intravascular brachytherapy. *Med. Phys.* 25, 339–346.
- Thoms, M., 1996. The quantum efficiency of radiographic imaging with image plates. *Nucl. Instrum. Methods A* 378, 598–611.
- Winnacker, A., 1993. X-ray imaging with photostimulable storage phosphors and future trends. *Phys. Med.* IX (2–3), 95–101.
- Zhu, Y., Kirov, A.S., Mishra, V., Meigooni, A.S., Williamsom, J.F., 1997. Quantitative evaluation of radiochromic film response for two-dimensional dosimetry. *Med. Phys.* 24, 223–231.